Generalized sum rules of the nucleon in the constituent quark model

M. Gorchtein[1], D. Drechsel[2], M.M. Giannini[1], E. Santopinto[1] and L. Tiator[2]

April 6, 2004

[1] Università di Genova, Sezione INFN di Genova,
via Dodecaneso 33, 16146 Genova (Italy)
[2] Institut für Kernphysik, Universität Mainz,
J.-J.-Becherweg 45, 55099 Mainz (Germany)

Abstract

We study the generalized sum rules and polarizabilities of the nucleon in the framework of the hypercentral constituent quark model. We include in the calculation all the well known 3* and 4* resonances and consider all the generalized sum rules for which there are data available. To test the model dependence of the calculation, we compare our results to the results obtained in the harmonic oscillator CQM. We furthermore confront our results to the model-independent sum rules values and to the predictions of the phenomenological MAID model. The CQM calculations provide a good description of most of the presented generalized sum rules in the intermediate Q^2 region (above ~ 0.2 GeV^2) while they encounter difficulties in describing these observables at low Q^2, where the effects of the pion cloud, not included in the present calculation, are expected to be important.

1   Introduction

The sum rules for real and virtual Compton scattering are constructed as energy-weighted integrals over the various contributions to the inclusive cross section. We list the generalized sum rules in Section 2 and refer the reader to Refs. [1],[2] for details of the derivation. The sum rules serve as a powerful tool to study the nucleon structure by providing a bridge between the static properties of the nucleon (such as charge, mass, and magnetic moment) and the dynamical properties (e.g., the transition amplitudes to excited states) in a wide range of energy and momentum transfer Q^2. Since a constituent quark model (CQM) provides predictions for both the static and the dynamic properties, the sum rules make it possible to test the consistency of the model. Recently, precise measurements of the generalized

1

sum rules and related observables have become available in a series of experiments [3]-[8]. Furthermore, the MAID model [9], [10] yields a detailed analysis of the (mainly) single pion photo- and electroproduction channels in a wide energy and Q^2 range.

In recent years much attention has been devoted to the description of the internal nucleon structure in terms of constituent quark degrees of freedom. Besides the now classical Isgur-Karl model [11], the Constituent Quark Model has been proposed in quite different approaches: the Capstick and Isgur model [12], the chiral model [13], [14], the algebraic $U(7)$-model [15], and the hypercentral formulation [16].

In this work we study the generalized sum rules for the nucleon, briefly reviewed in Section 2, within the hypercentral constituent quark model. In Section 3, we discuss the main features of this model and obtain the expressions for the generalized sum rules within the zero-width approximation. For this calculation, we consistently use the parameters of the model fixed to the baryonic spectrum as given by previous publications [16]-[20]. In the past, a series of calculations were performed in various CQM models [21, 22], however all of them restricted themselves to the GDH sum rule only and had their scope in reproducing the value of this sum rule at $Q^2 = 0$. At finite values of the momentum transfer, the experimental data for the first moment of the proton DIS structure function g_1 were compared to the CQM calculation in Ref.[22]. Thanks to the availability of many new precise data for different generalized sum rules for both the proton and the neutron, we now attempt to provide a description of all the nucleon sum rules using the same model without any new ingredients as compared to the baryonic spectrum calculation. Since for the moment it is impossible to account for the $q\bar{q}$ (pionic) degrees of freedom in a model independent way, such contributions are not included in this work. In our calculation, we include the 14 well-known resonances (3* and 4* in the classification of PDG). To test the dependence on the particular quark model, we also consider the harmonic oscillator type of the CQM. In Section 4, we present our predictions for the generalized sum rules for the proton and neutron and compare them to the available data. Finally, in Appendix A, we provide details of the derivation of the inclusive cross sections in the helicity representation.

2 Generalized sum rules

The inclusive cross section for electron-proton scattering can be written as follows:

$$\frac{d\sigma}{d\Omega dE'} = \Gamma_V \left[\sigma_T + \epsilon\sigma_L - hP_z\sqrt{1-\epsilon^2}\sigma_{TT} - hP_x\sqrt{2\epsilon(1-\epsilon)}\sigma_{LT} \right] \quad (1)$$

with the virtual photon flux factor

$$\Gamma_V = \frac{\alpha_{em}}{2\pi^2}\frac{E'}{E}\frac{K}{Q^2}\frac{1}{1-\epsilon} \, , \quad (2)$$

and the photon polarization

$$\epsilon = \frac{1}{1 + 2(1 + \nu^2/Q^2)\tan^2(\Theta/2)} \; , \tag{3}$$

where $E(E')$ denote the initial (final) electron energy, $\nu = E - E'$ the energy transfer to the target, Θ the electron scattering angle, and $Q^2 = 4EE'\sin^2(\Theta/2)$ the four-momentum transfer. The virtual photon spectrum normalization factor is chosen according to Hand's definition, $K = K_H \equiv \nu - \frac{Q^2}{2M}$, with M the nucleon mass. Furthermore, the polarization in Eq.(1) is described by the helicity of the electron, $h = \pm 1$, while P_z and P_x are the components of the target polarization along the virtual photon momentum and perpendicularly to it in the leptonic plane. The partial cross sections are related to the nucleon structure functions,

$$\sigma_T = \frac{4\pi^2\alpha_{em}}{MK} F_1 \; ,$$

$$\sigma_{TT} = \frac{4\pi^2\alpha_{em}}{MK} (g_1 - \gamma^2 g_2) \; ,$$

$$\sigma_L = \frac{4\pi^2\alpha_{em}}{K} \left\{ \frac{1 + \gamma^2}{\gamma^2} \frac{F_2}{\nu} - \frac{F_1}{M} \right\} \; ,$$

$$\sigma_{LT} = \frac{4\pi^2\alpha_{em}}{MK} \gamma (g_1 + g_2) \; , \tag{4}$$

with $\gamma = Q/\nu$.

The Baldin sum rule [23] relates the sum of the electric polarizability α and the magnetic susceptibility β to the following energy weighted integral over the total photoabsorption cross section:

$$\alpha(Q^2) + \beta(Q^2) = \frac{1}{2\pi^2} \int_{\nu_0}^{\infty} \frac{K(\nu, Q^2)}{\nu} \frac{\sigma_T(\nu, Q^2)}{\nu^2} d\nu \; , \tag{5}$$

where ν_0 is the threshold energy for pion production. Another sum rule expresses the longitudinal polarizability α_L by an integral over the longitudinal cross section σ_L [1],

$$\alpha_L(Q^2) = \frac{1}{2\pi^2} \int_{\nu_0}^{\infty} \frac{K(\nu, Q^2)}{\nu} \frac{\sigma_L(\nu, Q^2)}{\nu^2} d\nu \; . \tag{6}$$

The forward spin polarizability γ_0 can be calculated from the helicity difference σ_{TT},

$$\gamma_{TT}(Q^2) = \frac{1}{2\pi^2} \int_{\nu_0}^{\infty} \frac{K(\nu, Q^2)}{\nu} \frac{\sigma_{TT}(\nu, Q^2)}{\nu^3} d\nu \; . \tag{7}$$

Similarly, we obtain the longitudinal-transverse polarizability δ_{LT} from the integral

$$\delta_{LT}(Q^2) = \frac{1}{2\pi^2} \int_{\nu_0}^{\infty} \frac{K(\nu, Q^2)}{\nu} \frac{\sigma_{LT}(\nu, Q^2)}{Q\nu^2} d\nu \; . \tag{8}$$

3

Further sum rules are given by generalizations of the GDH sum rule [24], the purely transverse expression

$$I_{TT}(Q^2) \;=\; \frac{M^2}{\pi e^2} \int_{\nu_0}^{\infty} \frac{K(\nu, Q^2)}{\nu} \, \frac{\sigma_{TT}(\nu, Q^2)}{\nu} d\nu \;,$$ (9)

and the first moment of the structure function g_1 known from deep inelastic scattering (DIS),

$$I_1^N(Q^2) \;=\; \frac{2M^2}{Q^2} \int_0^{x_0} g_1^N dx \;=\; \frac{M^2}{\pi e^2} \int_{\nu_0}^{\infty} \frac{K}{\nu^2 + Q^2} \left[\sigma_{TT} + \frac{Q}{\nu} \sigma_{LT} \right] d\nu$$

$$\rightarrow \begin{cases} -\frac{\kappa_N^2}{4}, \; Q^2 \rightarrow 0 \\ \frac{2M^2}{Q^2} \Gamma_1^N, \; Q^2 \rightarrow \infty \end{cases}$$

where $\Gamma_1^N = \int_0^1 dx g_1^N(x, Q^2)$ and $x_0 = Q^2/(2M\nu_0)$.

The Bjorken sum rule [25] deals with the isovector combination of I_1,

$$\Gamma_1^p - \Gamma_1^n \;=\; \int_0^1 dx \left[g_1^p(x, Q^2) - g_1^n(x, Q^2) \right] \;\rightarrow\; \frac{1}{6} g_A \text{ at } Q^2 \rightarrow \infty \;,$$ (10)

with $g_A = 1.26$ the axial coupling constant of the nucleon. This sum rule is well established both theoretically and experimentally, i.e., at $Q^2 = 5$ GeV,

$$(\Gamma_1^p - \Gamma_1^n)^{exp} \;=\; 0.176 \pm 0.003 \pm 0.007 \quad [26]$$
$$(\Gamma_1^p - \Gamma_1^n)^{th} \;=\; 0.182 \pm 0.005 \quad [27] \;,$$ (11)

where the theoretical value contains the radiative corrections to Eq.(10).

In a similar way the Burkhardt-Cottingham (BC) sum rule [28] involves the first moment of the (DIS) structure function g_2. The BC sum rule states that this moment vanishes if integrated over elastic and inelastic contributions,

$$\int_0^1 g_2 dx \;=\; 0 \text{ for any } Q^2 \;.$$ (12)

If this relation holds, the inelastic contribution to the integral can be expressed by the nucleon form factors for all values of Q^2,

$$I_2(Q^2) \;=\; \frac{2M^2}{Q^2} \int_0^{x_0} g_2 dx \;=\; \frac{M^2}{\pi e^2} \int_{\nu_0}^{\infty} \frac{K}{\nu^2 + Q^2} \left[-\sigma_{TT} + \frac{\nu}{Q} \sigma_{LT} \right] d\nu$$

$$= \; \frac{1}{4} \frac{G_M(Q^2)(G_M(Q^2) - G_E(Q^2))}{1 + Q^2/4M^2} \;.$$ (13)

Furthermore, if we add the integrals I_1 and I_2, we obtain the purely longitudinal-transverse expression

$$I_{LT}(Q^2) = \frac{M^2}{\pi e^2} \int_{\nu_0}^{\infty} \frac{K(\nu, Q^2)}{\nu} \frac{1}{Q} \sigma_{LT}(\nu, Q^2) d\nu \;.$$ (14)

At the real photon point, $Q^2 = 0$, the values of the sum rules take the following values [1]:

$$
\begin{aligned}
\alpha^p(0) + \beta^p(0) &= 13.69 \cdot 10^{-4} fm^3 \quad [29] \, , \\
\alpha_L(0) &= 0 \\
\gamma^p_{TT}(0) &= -1.01 \cdot 10^{-4} fm^4 \quad [3] \\
I_{TT}(0) &= -\frac{\kappa_N^2}{4} \\
I_1(0) &= -\frac{\kappa_N^2}{4} \\
I_2(0) &= \frac{\kappa_N(e_N + \kappa_N)}{4} \\
I_{LT}(0) &= \frac{e_N \kappa_N}{4} \, ,
\end{aligned}
\tag{15}
$$

with $e_p = 1$, $e_n = 0$, $\kappa_p = 1.79$, $\kappa_n = -1.91$.

3 Constituent quark model

In the following we shall review the hypercentral Constituent Quark Model (HCQM), which has been used for a systematic calculation of various baryon properties.

The experimental 3^* and 4^* non strange resonances can be arranged in $SU(6)-$multiplets. This means that the quark dynamics has a dominant $SU(6)-$ invariant part, which accounts for the average multiplet energies. In the HCQM the potential is assumed to take the form [16]

$$
V(x) = -\frac{\tau}{x} + \alpha x \, ,
\tag{16}
$$

with the hyperradius $x = \sqrt{\vec{\rho}^2 + \vec{\lambda}^2}$, where $\vec{\rho}$ and $\vec{\lambda}$ are the Jacobi coordinates describing the internal quark motion. We note that the "hypercentral" potential does not depend on the hyperangle $\xi = arctg(\rho/\lambda)$.
Interactions of the type linear plus Coulomb-like have been used for a long time in the meson sector, e.g. the Cornell potential. This form has been supported by recent Lattice QCD calculations [30].
In the case of baryons a so called hypercentral approximation was introduced [31], which amounts to average any two-body potential for the three quark system over the hyperangle ξ. This approximation works quite well, especially for the lower part of the spectrum [32]. In this respect, the hypercentral potential Eq.(16) can be considered as the hypercentral approximation of a two-body Coulomb-like plus linear confining potential.

The hypercoulomb term $1/x$ has important features [16, 33]: it can be solved analytically and the resulting form factors have a power-law behaviour, at variance with the widely used harmonic oscillator. Moreover,

the negative parity states are exactly degenerate with the first positive parity excitation, which provides a good starting point for the description of the spectrum.

The splittings within the multiplets are produced by a perturbative term breaking the $SU(6)$ symmetry, which, as a first approximation, can be assumed to be the standard hyperfine interaction H_{hyp} [11]. The three quark hamiltonian for the HCQM is then:

$$H = \frac{p_\lambda^2}{2m} + \frac{p_\rho^2}{2m} - \frac{\tau}{x} + \alpha x + H_{hyp}, \qquad (17)$$

where m is the quark mass (taken equal to $1/3$ of the nucleon mass). The strength of the hyperfine interaction is determined such as to reproduce the $\Delta - N$ mass difference, the two remaining free parameters are fitted to the spectrum, which yields the following values:

$$\alpha = 1.61 \ fm^{-2}, \qquad \tau = 4.59 \ . \qquad (18)$$

Keeping these parameters fixed, the model has been applied to calculate various physical quantities of interest: the photocouplings [17], electromagnetic transition amplitudes [18], the elastic nucleon form factors [19], in particular the ratio between the electric and magnetic form factors, and recently in a systematic calculation of the longitudinal electromagnetic form factors for all the 3^* and 4^* resonances [34].

We also observe that the harmonic oscillator potential, which is widely used in quark models because of its analytical solution, is in fact exactly hypercentral,

$$\sum_{i<j} \frac{1}{2}k(\vec{r}_i - \vec{r}_j)^2 \ = \ \frac{3}{2}kx^2 \ = \ V_{HO}(x) \ , \qquad (19)$$

and thus can be treated in the hypercentral approach.

For comparison, we shall also show the analytical results within the constituent quark model with the harmonic oscillator potential (HO) of Ref. [11], which gives analytical results for the transverse helicity amplitudes $A_{1/2}$ and $A_{3/2}$. The results for the longitudinal helicity amplitudes $S_{1/2}$ are constructed in a similar way. We now relate the partial cross sections to the helicity amplitudes for resonance excitation. In the following we use the *lab* frame with the proton four-momentum $p^\mu = (M, \vec{0})$, and $q^\mu = (\nu, 0, 0, q)$ the four-momentum of the virtual photon. The photon polarization vectors take the form:

$$\begin{aligned}
\varepsilon^{(\pm)} &= \mp \frac{1}{\sqrt{2}}(0, 1, \pm i, 0) \\
\varepsilon^{(0)} &= \frac{1}{Q}(q, 0, 0, \nu) \ .
\end{aligned} \qquad (20)$$

6

The spherical components of the (three-vector) current are defined by $J_\pm = \mp(J_x \pm i\,J_y)/\sqrt{2}$ and $J_0 = J_z$. The latter is related to the charge by gauge invariance, $q \cdot J = \nu\rho - qJ_z = 0$. From these equations we find

$$
\begin{aligned}
\varepsilon^{(\pm)} \cdot J &= -J_\pm \ , \\
\varepsilon^{(0)} \cdot J &= \frac{Q}{\nu}\, J_0 = \frac{Q}{q}\rho \ ,
\end{aligned} \tag{21}
$$

which leads to a Lorentz invariant description of the transition operators. The electromagnetic transition helicity amplitudes are then defined by

$$
\begin{aligned}
A_{1/2} &= -\frac{e}{\sqrt{2K}} < R, \frac{1}{2}|J_+|N, -\frac{1}{2} > \xi \ , \\
A_{3/2} &= -\frac{e}{\sqrt{2K}} < R, \frac{3}{2}|J_+|N, \frac{1}{2} > \xi \ , \\
S_{1/2} &= -\frac{e}{\sqrt{2K}} < R, \frac{1}{2}|\rho|N, \frac{1}{2} > \xi \ ,
\end{aligned} \tag{22}
$$

where the 3rd component of the nucleon and resonance spins are explicitly indicated. The phases ξ depend on the strong decay matrix elements, which have to be individually calculated in the respective model. In comparing with Eq. (21), we note that the $S_{1/2}$ amplitude is finite at the real photon point ($Q^2 = 0$). However, only the product $\frac{Q}{q} S_{1/2}$ transforms as a Lorentz scalar. A single resonance contribution to the transverse helicity cross sections is given by [35]

$$
\sigma_\Lambda = \frac{4M}{M_R\Gamma_R}|A_\Lambda|^2 \ , \quad \Lambda = \frac{1}{2} \text{ or } \frac{3}{2} \ , \tag{23}
$$

with M_R and Γ_R the mass and the full width of the resonance. The total photoabsorption cross section σ_T and the helicity difference σ_{TT} are then obtained by

$$
\begin{aligned}
\sigma_T &= \frac{\sigma_{1/2} + \sigma_{3/2}}{2} = \frac{2M}{M_R\Gamma_R}\left\{|A_{1/2}|^2 + |A_{3/2}|^2\right\} \ , \\
\sigma_{TT} &= \frac{\sigma_{1/2} - \sigma_{3/2}}{2} = \frac{2M}{M_R\Gamma_R}\left\{|A_{1/2}|^2 - |A_{3/2}|^2\right\} \ .
\end{aligned} \tag{24}
$$

The helicity amplitudes for the transitions $\gamma^* N \to R$ can be directly calculated within the CQM at the resonance position in the limit of a sharp resonance. In this limit, the energy dependence of the cross section is described by a δ-function. In a more realistic scenario we describe a resonance with a finite width Γ_R and a resonance energy M_R, such that the real part of the amplitude vanishes exactly at resonance,

$$
A_\Lambda(W) = \frac{\Gamma_R/2}{W - M_R - i\Gamma_R/2}\, A_\Lambda^0 \ , \tag{25}
$$

where $W = \sqrt{2M\nu + M^2 - Q^2}$ is the total *c.m.* energy and A_Λ^0 the helicity amplitude as calculated in the CQM. We note that these CQM helicity amplitudes can be defined to be real by choice of the model-dependent phases ξ introduced in Eq.(22), and therefore we shall treat these amplitudes as real numbers in the following equations. Using equations (23) and (25), we obtain the cross section in the zero-width approximation, in the limit $\Gamma_R \to 0$,

$$\sigma_\Lambda^0(W) = 2\pi\delta(W - M_R)\frac{M}{M_R}(A_\Lambda^0)^2 . \tag{26}$$

Expressed as function of the photon *lab* energy ν, the zero-width cross section takes the form

$$\sigma_\Lambda^0(\nu) = 2\pi\delta(\nu - \nu_R)(A_\Lambda^0)^2 , \qquad \Lambda = \frac{1}{2} \text{ and } \frac{3}{2}$$

$$\sigma_L^0(\nu) = 2\pi\delta(\nu - \nu_R)\left(\frac{Q}{q_R}\right)^2(S_{1/2}^0)^2 ,$$

$$\sigma_{LT}^0 = -\sqrt{2}\pi\delta(\nu - \nu_R)\frac{Q}{q_R}S_{1/2}^0 A_{1/2}^0 . \tag{27}$$

Since the sign of the longitudinal-transverse interference term is not uniquely defined in the literature, we address the reader to Appendix A for a derivation of the inclusive cross section in the helicity formalism. We are now in a position to express the sum rules of the previous section in terms of the helicity amplitudes in the zero-width approximation:

$$I_{TT}(Q^2) = \frac{M^2}{e^2} \sum_R \frac{K}{\nu_R^2} \left[(A_{R\frac{1}{2}}^0)^2 - (A_{R\frac{3}{2}}^0)^2\right] , \tag{28}$$

$$I_1(Q^2) = \frac{M^2}{e^2} \sum_R \frac{K}{q_R^2} \left\{(A_{R\frac{1}{2}}^0)^2 - (A_{R\frac{3}{2}}^0)^2 - \frac{\sqrt{2}Q^2}{\nu_R q_R}S_{R\frac{1}{2}}^0 A_{R\frac{1}{2}}^0\right\} , \tag{29}$$

$$I_2(Q^2) = \frac{M^2}{e^2} \sum_R \frac{K}{q_R^2} \left\{(A_{R\frac{3}{2}}^0)^2 - (A_{R\frac{1}{2}}^0)^2 - \sqrt{2}\frac{\nu_R}{q_R}S_{R\frac{1}{2}}^0 A_{R\frac{1}{2}}^0\right\} , \tag{30}$$

$$I_{LT}(Q^2) = -\frac{\sqrt{2}M^2}{e^2} \sum_R \frac{K}{\nu_R q_R} S_{R\frac{1}{2}}^0 A_{R\frac{1}{2}}^0 , \tag{31}$$

$$\alpha(Q^2) + \beta(Q^2) = \frac{1}{2\pi} \sum_R \frac{K}{\nu_R^3} \left\{(A_{R\frac{1}{2}}^0)^2 + (A_{R\frac{3}{2}}^0)^2\right\} , \tag{32}$$

$$\alpha_L(Q^2) = \frac{1}{\pi} \sum_R \frac{K}{\nu_R^3}\frac{Q^2}{q_R^2}(S_{R\frac{1}{2}}^0)^2 , \tag{33}$$

$$\gamma_{TT}(Q^2) = \frac{1}{2\pi} \sum_R \frac{K}{\nu_R^4} \left\{(A_{R\frac{1}{2}}^0)^2 - (A_{R\frac{3}{2}}^0)^2\right\} , \tag{34}$$

8

$$\delta_{LT}(Q^2) = -\frac{1}{\sqrt{2}\pi} \sum_R \frac{K}{\nu_R^3 q_R} S^0_{R\frac{1}{2}} A^0_{R\frac{1}{2}}, \tag{35}$$

where $K = K(\nu_R, Q^2)$.

4 Results

In this section we present our results for the generalized nucleon sum rules obtained with the following 14 resonances (3^* and 4^* in the PDG classification): $P_{33}(1232)$, $P_{11}(1440)$, $S_{11}(1535)$, $D_{13}(1520)$, $S_{31}(1620)$, $S_{11}(1650)$, $D_{15}(1675)$, $F_{15}(1680)$, $P_{11}(1710)$, $D_{33}(1700)$, $P_{13}(1720)$, $D_{13}(1700)$, $F_{35}(1905)$, $F_{37}(1950)$.

4.1 Generalized GDH integrals

We start with the results for the integrals I_1^p and I_{TT}^n, for which experimental data are available. In Fig. 1, we show the predictions of the two CQMs for $I_1^p(Q^2)$ together with the MAID results, and confront them to the experimental data of Refs. [4] - [6].
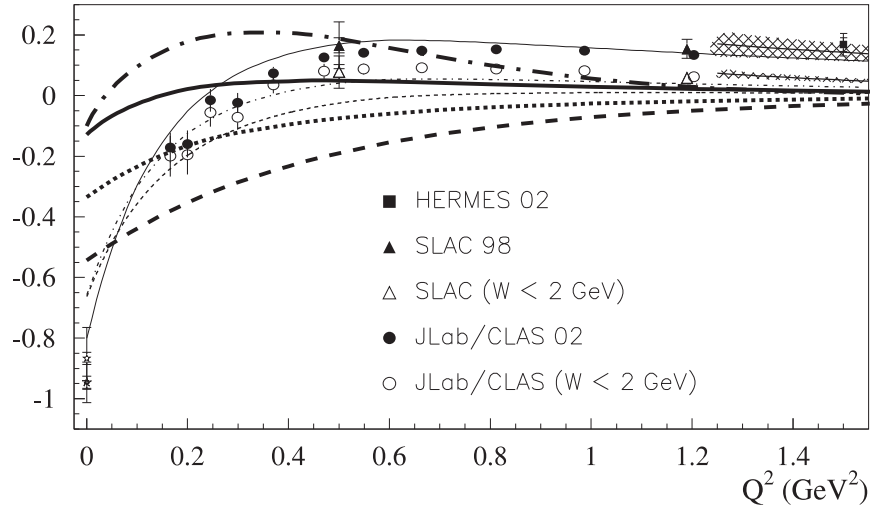
Figure 1: Predictions of the HCQM and HO models for the integral I_1^p as compared to the MAID results. The HCQM results are shown for the $\Delta(1232)$ only (thick dashed line), $\Delta(1232)$ plus negative parity resonances (thick dotted line), and including all 3^* and 4^* resonances (thick solid line). For the HO model, we only show the full result (thick dash-dotted line). The thin dashed line corresponds to MAID (one-pion contribution only). The thin dash-dotted line corresponds to MAID with one and two-pion contributions. The thin solid line shows the phenomenological parametrization of Ref. [36]. The solid circles (Ref. [6]), solid triangles (Ref. [4]), and solid squares (Ref. [5]) correspond to the evaluation of the integral over the full energy range, while the open circles (Ref. [6]) and open triangles (Ref. [4]) include the resonance region only ($W < 2$ GeV). For the JLab data [6], only the statistical errors are shown. The solid lines with shaded bands starting at 1.25 GeV^2 represent the evaluation with the data for the structure function g_1, integrated over the full energy range (upper band) and over the resonance region only ($W < 2$ GeV, lower band), including the corresponding error estimates [37].

In the range of momentum transfer $0.3 < Q^2 < 0.6$ GeV^2, the HCQM results are compatible with the experimental data evaluated over the "resonance" region ($W \leq 2$ GeV) but show not enough structure in Q^2 to reproduce the data over the full range of the momentum transfer shown. However, we find a notable agreement between the HCQM and MAID with one and two-pion contributions starting from $Q^2 = 0.5$ GeV^2, where the effects of the pion cloud, included in MAID but absent in the quark model, are less important than at low momentum transfers. At $Q^2 = 0$, however, both CQ models fail to reproduce the sum rule value. We shall come back to this point later.

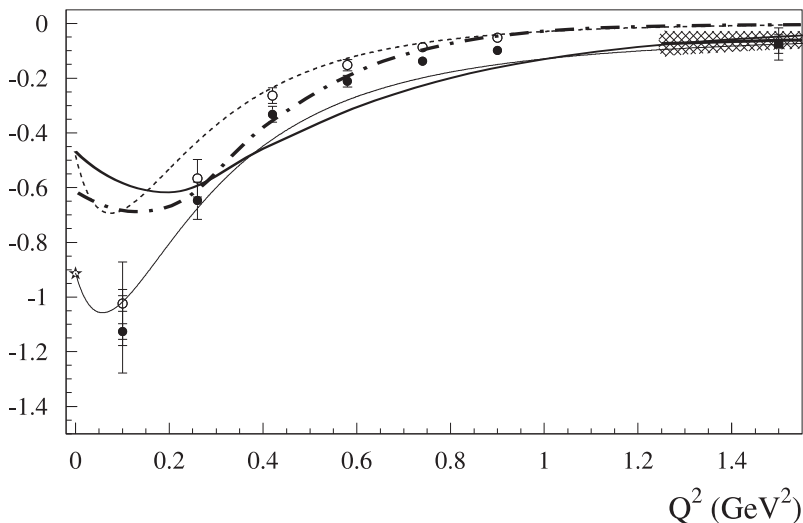Next we present the results for the purely transverse neutron integral I_{TT}^n in Fig. 2.

Figure 2: The CQM predictions for the GDH integral on the neutron, I_{TT}^n. The data points are from Refs. [5] (solid squares) and [7] with the nuclear corrections included (solid circles) [38] and without these corrections (open circles). The curves represent the results of HCQM (thick solid), HO (dashed-dotted), MAID (dashed), and the parametrization of [36] (thin solid), fitted to the sum rule value at $Q^2 = 0$ (solid star).

Again, the two quark models underestimate the strength in the low Q^2 region. Since the effect of the negative parity resonances is nearly zero in the neutron case, the only significant deviation from the pure $\Delta(1232)$ contribution comes from the Roper. Due to characteristic Gaussian form factors, the HO model is able to reproduce the data only up to $Q^2 \approx 1$ GeV^2, but falls short of the data beyond this region. On the contrary, the HCQM prediction decreases significantly slower with increasing Q^2, as compared to the HO model. However, for $Q^2 > 0.4$ GeV^2 it follows the phenomenological fit of Ref. [36] and is in very good agreement with the evaluation

of the I^n_{TT} integral with the DIS data and the data point from Ref. [5].

We conclude that the presented CQM does not provide a satisfactory description of the GDH sum rule at $Q^2 = 0$. The reason for this is the fact that the strength at low Q^2 is underestimated for the $\Delta(1232)$ case, which gives the dominant contribution, and similarly for most of the higher resonances. This indicates the importance of other contributions, such as the pion cloud effects, not only for the background but for the $N + \gamma \to N^*$ transitions as well. In this respect, it is interesting to note that for I^p_1, the HCQM and MAID results coincide over a large range of intermediate Q^2 values, while they differ at low momentum transfer values, where the pion loop effects are important.

Although the integral I_1 contains a contribution of the longitudinal-transverse term, this latter vanishes at the real photon point, and therefore the disagreement at $Q^2 = 0$ is due to the purely transverse resonance contributions. We can learn more about this fact by studying another integral containing the helicity cross section difference, i.e. the forward spin polarizability γ_{TT}.

4.2 Forward spin polarizability

Figure 3 shows the CQM results and the MAID predictions for the generalized forward spin polarizability γ_{TT} of the proton. The left panel shows this observable directly, while the right panel includes an appropriate factor to make contact with the moments of g_1 and g_2,

$$\frac{Q^6}{4M^2}\gamma_{TT} \;=\; \frac{e^2}{\pi} \int_0^{x_0} x^2(g_1 - \frac{4M^2}{Q^2}x^2 g_2)dx \; . \tag{36}$$

In this sum rule, there are two more powers of the energy in the denominator than in the GDH integral, such that the low lying resonances are more emphasized as compared to the higher resonances than in the case of the GDH. In fact, it is an easy excercise to prove that if the GDH sum rule is described by the $\Delta(1232)$ alone, this would result in a value of $\gamma_{TT}(GDH \equiv \Delta) \approx -1.73 \cdot 10^{-4}$ fm^4, which is much below the experimental data, see Eq.(15). Within a phenomenological analysis like MAID, one finds that the rather small sum rule value for γ_{TT} comes about due to a destructive interference of large contributions of the $\Delta(1232)$ resonance and s-wave pion production near threshold. Of course, the pion cloud also contributes to the GDH integral, but with a much smaller impact due to the different energy weighting. As can be seen from Fig. 3, both quark models provide fairly good descriptions for γ_{TT} at $Q^2 = 0$. The absence of the pion threshold production in the CQM is compensated by the destructive interference effects of higher resonances and a lack of strength in the resonance region, which can also be ascribed to a lack of the pion cloud in these transitions.
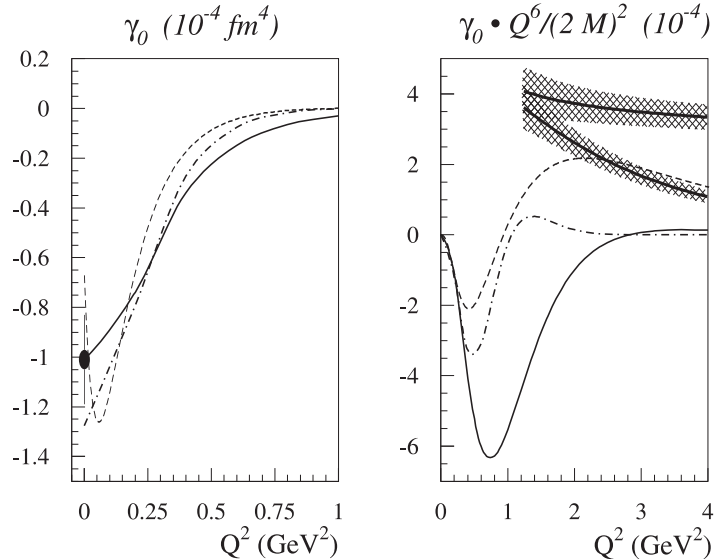
Figure 3: Predictions for the generalized proton forward spin polarizability γ_{TT} in units of $10^{-4}fm^4$ (left panel) and $\gamma_{TT} \cdot (Q^6/(2M)^2)$ in units of 10^{-4} (right panel) within the HCQM (solid lines) and the HO (dashed-dotted lines) predictions in comparison with the MAID results for the one-pion contribution only [10] (dashed lines). The data point is from Ref. [3]. The shaded bands in the right panel show the evaluation of Eq.(36) with the DIS results for the structure functions g_1 and g_2, integrated over the full energy range (upper band) and over the resonance region only ($W < 2$ GeV, lower band).

4.3 Baldin sum rule

We proceed with the Baldin sum rule which puts a constraint on the sum of the contributions from the $J = \frac{1}{2}$ and $J = \frac{3}{2}$ channels instead of their difference, as in the case of the sum rules discussed before.

In Fig. 4, we compare the CQM results with the MAID prediction for the Baldin sum rule of the proton. While the left panel displays $\alpha + \beta$ directly, the right panel shows this observable with an appropriate factor to obtain the lowest moment of the DIS structure function F_1,

$$\frac{Q^4}{2M}(\alpha + \beta) = \frac{e^2}{\pi} \int_0^{x_0} xF_1(x, Q^2)dx . \tag{37}$$

At $Q^2 = 0$, both CQM models lack considerable strength, which again can be explained by the absence of the pion cloud contribution in these models. Due to the energy weighting of the integrals with $1/\nu^2$, the long-range pion contribution is dominant at low Q^2 but decreases with Q^2 substantially faster than the resonance contribution. At larger values of Q^2, the HO results are practically zero above $Q^2 = 2$ $(\text{GeV/c})^2$, due to the strong Gaussian form factor of the HO potential, while the HCQM curves agree reasonably well with the "resonant DIS" and MAID results. However, the gap between those predictions and the full integral evaluated with
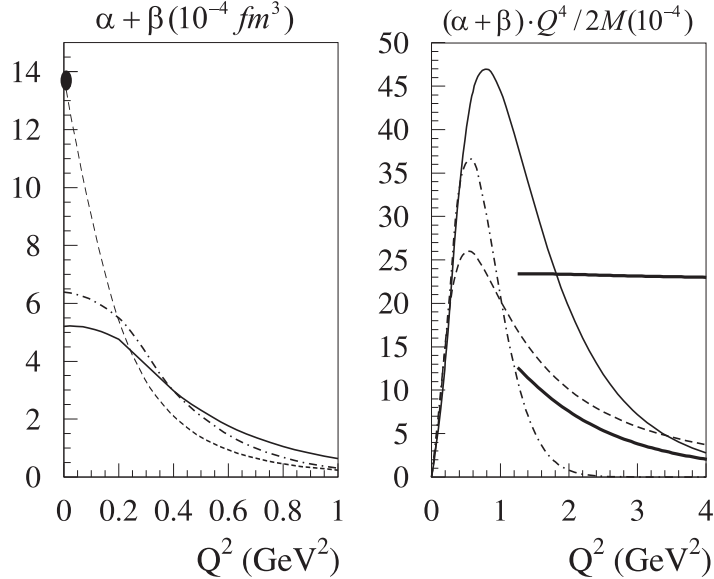
13

Figure 4: Predictions for the generalized proton polarizability $(\alpha + \beta)$ in units of $10^{-4} fm^3$ (left panel) and $(\alpha + \beta) \cdot (Q^4/2M)$ in units of 10^{-4} (right panel) within HCQM (solid lines) and HO (dashed-dotted lines) in comparison with the MAID results including the two-pion contribution [10] (dashed lines). The solid circle corresponds to the evaluation of the Baldin sum rule by Ref. [29]. The thick solid lines in the right panel are obtained by evaluating Eq.(37) with the DIS structure function F_1^p, integrated over the full spectrum (upper curve) and over the resonance region only (lower curve, $W \leq 2$ GeV).

the DIS structure function F_1 indicates that all the models lack important contributions in this Q^2 range due to the neglect of the contributions above $W = 2$ GeV.

Combining the information from the discussed integrals, we find that the description of the GDH sum rule with the $\Delta(1232)$ resonance alone, which has been widely used in the literature [21], turns out to be inconsistent for the other sum rules, since it leads to an overestimate of γ_{TT} by about a factor of 2 and an even more dramatic underestimation of the Baldin sum rule. In order to correctly reproduce all the sum rules for transverse photons at $Q^2 = 0$, one needs a contribution below the $\Delta(1232)$ resonance, which affects the various sum rules in a different way, because of the respective weighting factors $(1/\nu, /\nu^2$ and $1/\nu^3)$ involved. Unfortunately, at present no formalism exists which would allow for an inclusion of such $q\bar{q}$ ("pionic") effects in a model independent way. However, at higher values of the momentum transfer, such mechanisms become less important and as a result, the HCQM is able to reproduce the experimental data in the range 0.2 GeV^2 < Q^2 < 1.5 GeV^2. The applicability of the CQM

with the HO nucleon wave functions is however restricted to momentum transfers below 1 GeV^2, because of its Gaussian form factors.

4.4 Bjorken sum rule

In Fig. 5, we study the isovector combination of I_1, which is fixed by the Bjorken sum rule for $Q^2 \to \infty$. Unlike the MAID model with the one-pion contribution only, which in this case gives the wrong sign of the sum rule, the two CQM models predict the right sign of this sum rule but overestimate its value, which is of course due to the failure to reproduce the GDH sum rule. Clearly, the isovector integral is only sensitive to the N^* resonances and not to the Δ resonances, which contribute equally for proton and neutron. At 0.5 GeV$^2 < Q^2 < 1.2$ GeV^2, the HCQM model reproduces the "resonant" SLAC and JLab data nicely, while the HO model drops too fast due to its Gaussian form factors.
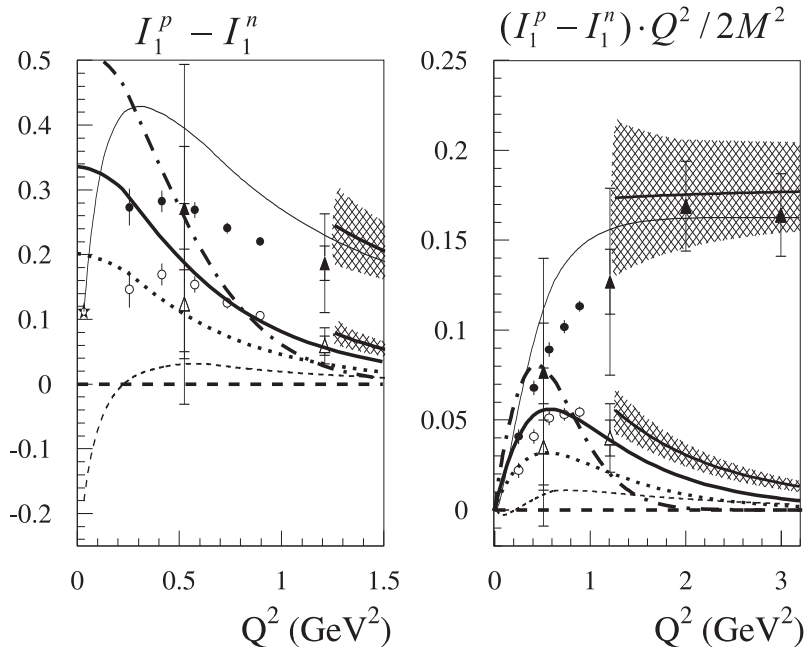

Figure 5: The isovector integral $I_1^p - I_1^n$ as calculated in the HCQM and HO models in comparison with the MAID results and the Bjorken sum rule. The solid and open triangles are data from Ref. [4]. The solid and open circles represent the combined proton data from [6] and neutron data from [8], with only statistical errors shown. The sum rule value is given by the star at $Q^2 = 0$, and the thin solid line shows the parametrization of Ref. [36]. Further notation as in Fig. 1.

4.5 Burkhardt-Cottingham sum rule

The Burkhardt-Cottingham sum rule connects the I_2 integral over the excitation spectrum to the nucleon form factors for any value of Q^2. In Fig. 6, we compare the predictions of the HCQM and HO models for this integral with the results of MAID, and confront them with the sum rule. For the proton, MAID agrees within 10% accuracy with the sum rule already with one-pion contribution only, however from $Q^2 \sim 0.2$ GeV^2 it starts to deviate stronger. The two quark models agree over the shown range of Q^2, which implies that the first moment of g_2^p depends on the particular quark model only weakly. However, both quark models underestimate the sum rule significantly. In the case of the neutron, new experimental data on the ^{3}He target are available [8]. From the comparison to these data, we find a very good agreement of the HO results with these data and with MAID starting from 0.25 GeV^2. HCQM does agree qualitatively with the data over the same range as well but lacks structure in Q^2 for this observable.
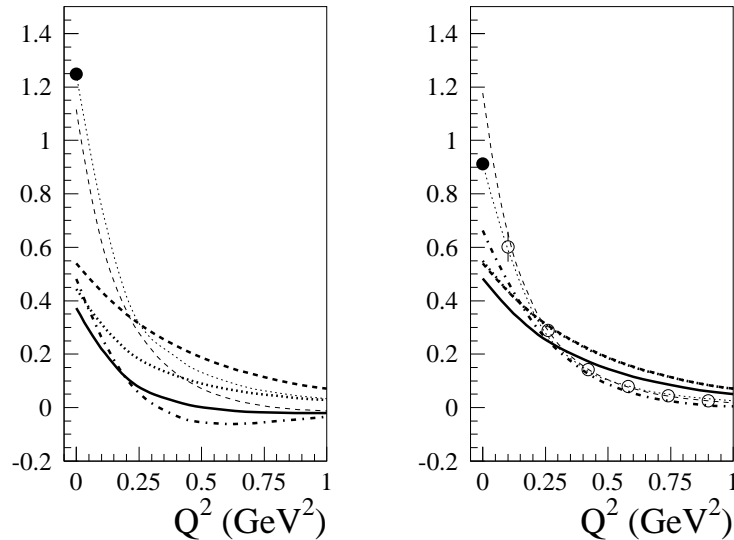

Figure 6: Results for the integral I_2 for proton (left panel) and neutron (right panel). The Burkhardt-Cottingham sum rule corresponds to the solid circles at $Q^2 = 0$ and the thin dotted lines. The data are from [8] (open circles) with only the statistical errors shown. Further notation as in Fig. 1.

4.6 Generalized I_{LT} integral

This sum rule deals with the sum of the first moments of the DIS structure functions g_1 and g_2,

$$I_{LT} \equiv I_1 + I_2 = \int_0^{x_0} (g_1(x, Q^2) + g_2(x, Q^2)) dx , \qquad (38)$$

and depends on the longitudinal-transverse interference term only. If the BC and the GDH sum rules hold, this integral is fixed at the real photon point,

$$I_{LT}(0) \;=\; \frac{e_N \kappa_N}{4} \; . \tag{39}$$

Our results for I_{LT} are shown in Fig. 7 for both proton and neutron.
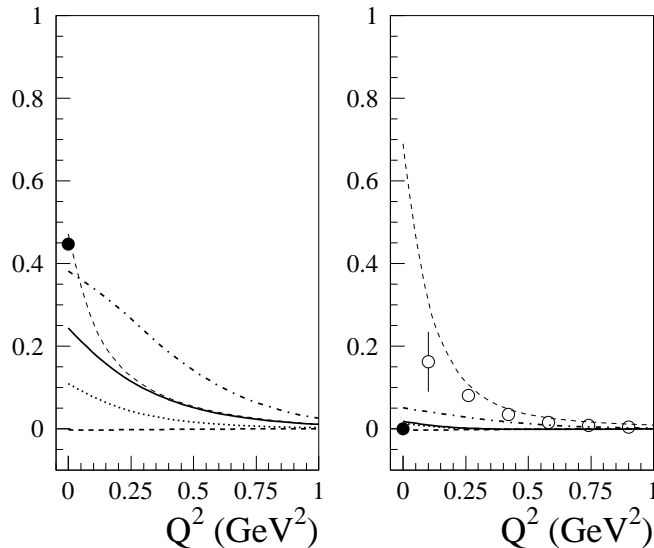

Figure 7: The integrals $I_{LT}(Q^2)$ for proton (left panel) and neutron (right panel) as calculated with the HCQM (solid lines) and the HO (dashed-dotted lines) models in comparison with the MAID results for the one-pion contribution (dashed lines). The solid circles represent the sum rule values. The data are from [8] (open circles) with only the statistical errors shown. Further notation as in Fig. 1.

In the case of the proton (left panel), the HO and MAID models agree reasonably well with Eq.(39), while the HCQM model lacks strength for this sum rule, which may be caused by the importance of the neglected pionic contributions. Starting from $Q^2 \approx 0.2$ GeV^2, beyond which region these contributions are less important, the HCQM is in notable agreement with MAID.
The situation is quite different for the neutron (right panel). In this case, MAID yields a large positive value at $Q^2 = 0$, while the sum rule requires $I_{LT}^n(0) = 0$. On the contrary, the HCQM result is in very good agreement with the sum rule, whereas the HO model gives a small positive value. At finite values of momentum transfer, the new data on $g_1^n + g_2^n$ shed more light on the situation with this sum rule, supporting the MAID predictions in the range $Q^2 > 0.2$ GeV^2. However, an inclusion of the non-resonant

17

contributions from energy range $W > 2$ GeV is necessary to match these data with the model-independent sum rule value and reduce the systematic errors (not displayed in Fig. 7).

The vanishing of $I_{LT}^n(0)$ requires, of course, an exact cancellation of all the resonance and background contributions. In order to track the mechanism of cancellations among the different resonances, the various contributions are separately displayed in Fig. 8, for both proton (solid lines) and neutron (dashed lines).
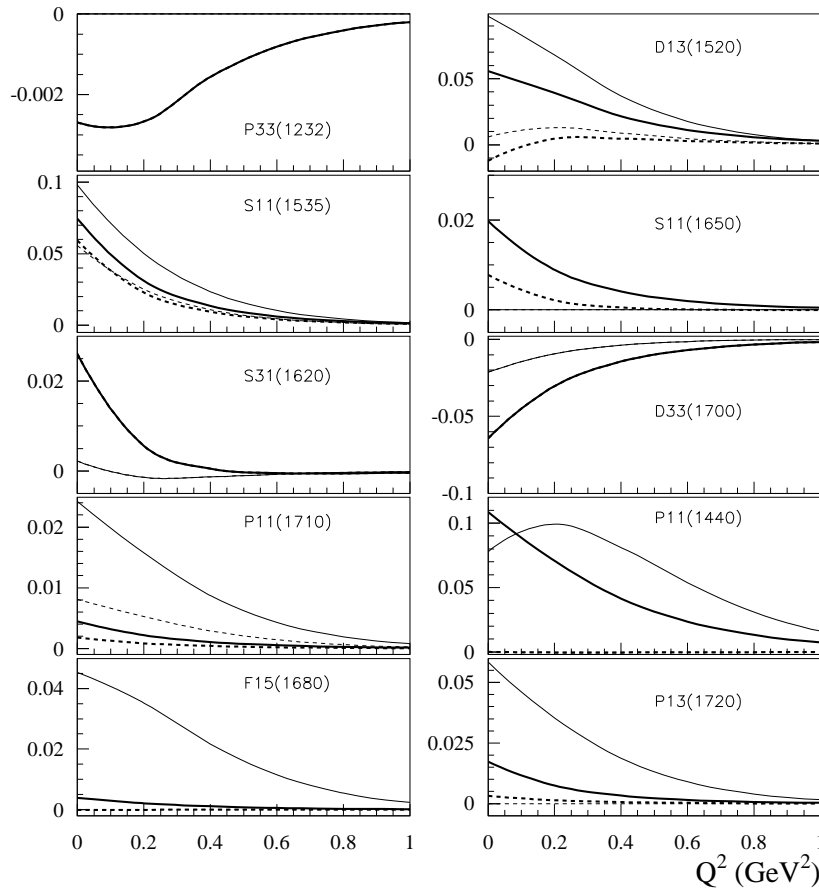

Figure 8: The single resonance contributions to the $I_{LT}(Q^2)$ integral as predicted by the HCQM for the proton (thick full lines) and for the neutron (thick dashed lines). The HO results are shown by the respective thin lines.

As can be clearly seen, the mechanism of this cancellation is quite different in the two models. In the case of HCQM, the major contributions are due to the resonances $D_{13}(1520)$, $P_{11}(1440)$, $S_{11}(1535)$, and $D_{33}(1700)$. The latter two cancel for both the proton and the neutron case. On the

other hand, the contributions of the resonances $D_{13}(1520)$ and $P_{11}(1440)$ are rather large for the proton but practically zero in the neutron case, which leads to a small sum rule value for the neutron. The presented HO calculation does not contain the $SU(6)$-breaking term, therefore most of the resonance contributions are zero in the case of the neutron. In the case of MAID, the failure to reproduce this zero may be related to the neglect of two-pion and heavier mass final states. However, it is even more likely that the discrepancy is due to the neglect of the spectrum above the $W = 2$ GeV, because I_{LT} clearly has the worst convergence of all the integrals.

4.7 Longitudinal-transverse polarizability δ_{LT}

We now discuss the polarizability δ_{LT} involving the longitudinal-transverse interference term σ_{LT} for the case of the proton. Figure 9 displays the predictions of the two CQMs in comparison with MAID. The latter predicts a large positive value for δ_{LT} at $Q^2 = 0$ due to the interference term $E_{0+} \cdot S_{0+}^*$, dominated by the near threshold s-wave pion production but absent in the CQM. However, starting from $Q^2 \approx 0.2$ GeV^2, the pionic contribution becomes small, and all the models give similar results. The right panel of Fig. 9 allows for a direct comparison to the integral evaluated with the DIS structure functions g_1 and g_2. As we can see, neither of the models matches to the DIS data, however the CQM models seem to work better in the range of 0.2 GeV$^2 < Q^2 < 2$ GeV^2.
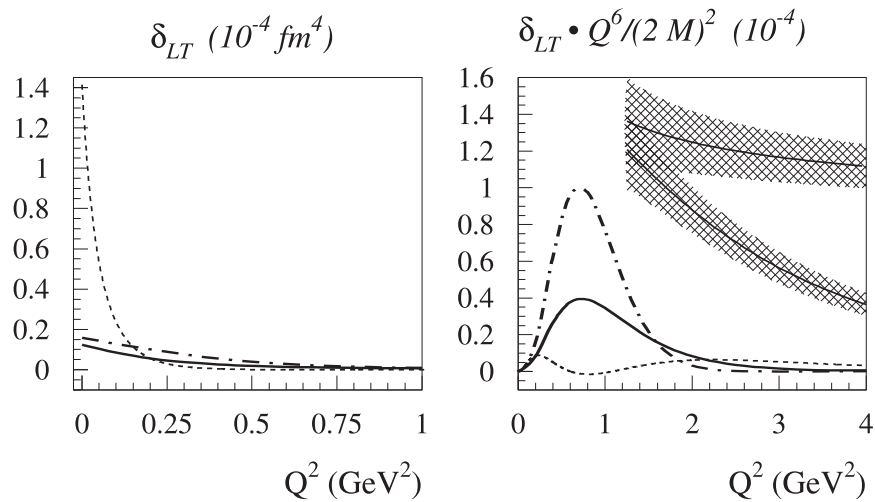

Figure 9: Results for δ_{LT}^p (left panel) in units of 10^{-4} fm^4, and $\delta_{LT} \cdot Q^6/(2M)^2$ in units of 10^{-4}. For further notation see Fig.3.

4.8 Longitudinal polarizability α_L

We finally show our results for the longitudinal polarizability α_L for the proton, in order to test our model for the purely longitudinal transitions. As becomes evident from Fig.10, all the presented models are incompatible with the DIS data over the full range covered by these data. This indicates that there is still space for further theoretical investigations of the longitudinal photon coupling to the nucleon.
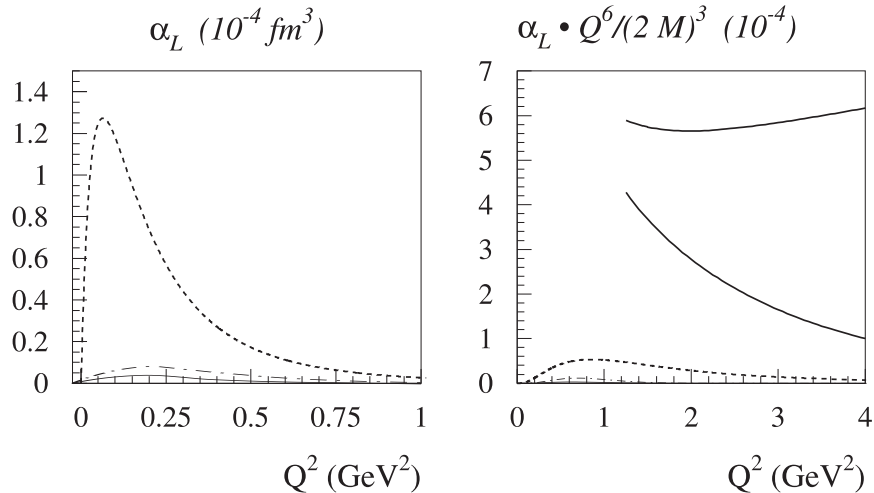

Figure 10: Results for α_L (left panel) in units of 10^{-4} fm^3, and $\alpha_L \cdot Q^6/(2M)^3$ in units of 10^{-4}. For further notation see Fig.3.

5 Conclusions

We have presented a calculation of the generalized sum rules and polarizabilities of the nucleon in the non-relativistic constituent quark model with the hypercentral potential. This model has been used previously to calculate various observables: the baryonic spectrum [16], the photocouplings [17], electromagnetic transition amplitudes [18], elastic nucleon form factors [19] and the longitudinal electromagnetic transition form factors [34]. The aim of these calculations was to consistently describe diverse observables within the same model, with all the parameters fixed to the spectrum, and the present work on the generalized sum rules is a further step in this direction. The generalized sum rules provide model-independent relations between the static and dynamic properties of the nucleon, and therefore only a model which correctly accounts for all the relevant mechanisms can be able to obey these sum rules. In the previous CQM calculations of the GDH sum rule [21] the emphasis was on the reproduction of the sum rule value at $Q^2 = 0$ which amounts to relating the anomalous magnetic moment of the nucleon to its excitation spectrum. However, in the last few

years a lot of experimental data have become available on the GDH and related sum rules over a wide range of Q^2, which allows us to test our model as function of the momentum transfer. In turn, this corresponds to testing the spatial distribution of the quark charge, spin, and momentum inside the nucleon. Since the CQM operates only with the heavy constituent quark degrees of freedom and neglects the quark-antiquark sea effects, it is expected that the model should experience difficulties at low Q^2 values, where these neglected effects become dominant. With the possible exception of γ_{TT}^p and $I_{LT}^n(0)$, our results clearly show that the CQM does not adequately describe the discussed integrals in the range $0 < Q^2 < 0.2$ GeV^2. We therefore conclude that the simple CQM description for the response of the nucleon to a quasistatic electromagnetic field is not adequate, and that an inclusion of the pionic ($q\bar{q}$) contributions is crucial in this kinematical region.

Such "pion cloud" effects are known to drop very fast with Q^2, and beyond $Q^2 \approx 0.2$ GeV^2, the HCQM agrees qualitatively with the corresponding integrals evaluated with the DIS structure function over the resonance region $W \leq 2$ GeV^2. For comparison, we plotted our predictions along with the predictions of the harmonic oscillator CQM and the phenomenological MAID model. The HO model gives very similar results as those of the HCQM at low Q^2, however it drops significantly faster with Q^2 due to its characteristic Gaussian form factors of the HO model, such that the observables are practically vanishing for $Q^2 \geq 1$ GeV^2. The MAID model accounts for all the leading mechanisms of pion production, such as resonant and non-resonant photo- and electroproduction, vector meson exchange, and uses extensive data sets to fix its parameters. For the proton, MAID works quite well at low and intermediate momentum transfers, but falls short of the data at the higher Q^2 values, which indicates increasing importance of the contributions above the resonance region. In the range of 0.2 GeV$^2 < Q^2 < 2$ GeV^2, we found that the HCQM model predicts most of the proton observables very similar to MAID. However, MAID fails to reproduce the neutron sum rules at the smaller momentum transfer, whereas the HCQM works for quite well in this case, especially for $I_{LT}(Q^2)$ and $I_{TT}(Q^2)$.

A Helicity representation of the inclusive cross section

In this appendix we derive the inclusive cross section of Eq.(1) for the scattering of an electron with definite helicity off a polarized nucleon characterized by its spin projection or helicity. Since we neglect the mass of

the electron, its helicity h cannot change in the scattering process. The hadronic transition leads from the nucleon with helicity Λ to an excited state with spin J and helicity Λ'. We note that all helicities are defined as projections of the spin on the direction of the virtual photon. The invariant matrix element for such a transition takes the form

$$
\begin{aligned}
T_{\Lambda' h' \Lambda h} &= \frac{e^2}{Q^2} \bar{u}(E', h') \gamma_\mu u(E, h) < J\Lambda' | J^\mu | \tfrac{1}{2}\Lambda > \\
&= \frac{e^2}{Q^2} \sum_\lambda \Omega_{h,\lambda} \delta_{h' h} < J\Lambda' | \varepsilon^{(\lambda)} \cdot J | \tfrac{1}{2}\Lambda > ,
\end{aligned}
\tag{40}
$$

where we inserted the complete set of polarization vectors of Eq. (20). The leptonic matrix element for a given helicity is

$$
\Omega_{h,\lambda} = \frac{\bar{u}(E', h') \varepsilon^{(\lambda)*} \cdot \gamma \, u(E, h)}{\varepsilon^{(\lambda)*} \cdot \varepsilon^{(\lambda)}} .
\tag{41}
$$

We evaluate this matrix element in the *lab* frame, choosing the x-z plane as the leptonic plane and with the virtual photon momentum $\vec{q}$ pointing in the direction of the z axis. The four-momenta of the electron are then given by

$$
\begin{aligned}
k^\mu &= E(1, \sin\Theta_1, 0, \cos\Theta_1) , \\
k'^\mu &= E'(1, \sin\Theta_2, 0, \cos\Theta_2) ,
\end{aligned}
\tag{42}
$$

with E and E' the initial and final electron energy, respectively, Θ_1 and Θ_2 the corresponding polar angles, and $\Theta = \Theta_2 - \Theta_1$ the scattering angle. The virtual photon has the four-momentum

$$
q^\mu = (\nu, 0, 0, |\vec{q}|) ,
\tag{43}
$$

where $\nu = E - E'$ and $Q^2 = \vec{q}^2 - \nu^2 > 0$.

The following kinematical relations are useful for the further calculation:

$$
\begin{aligned}
E \sin\Theta_1 &= E' \sin\Theta_2 = \frac{EE' \sin\Theta}{q} , \\
\cos\Theta_1 &= \frac{E - E' \cos\Theta}{q} , \\
\cos\Theta_2 &= \frac{E \cos\Theta - E'}{q} ,
\end{aligned}
\tag{44}
$$

The initial state electron spinor has the form

$$
u(E, h) = \sqrt{E} \begin{pmatrix} 1 \\ h \end{pmatrix} \chi_h ,
\tag{45}
$$

where χ_h is a Pauli spinor,

$$\chi_+ = \begin{pmatrix} \cos\frac{\Theta_1}{2} \\ \sin\frac{\Theta_1}{2} \end{pmatrix} \qquad \chi_- = \begin{pmatrix} -\sin\frac{\Theta_1}{2} \\ \cos\frac{\Theta_1}{2} \end{pmatrix} . \tag{46}$$

The final state spinor is then obtained by the replacement $E \to E'$, $h \to h'$, and $\Theta_1 \to \Theta_2$. We further note that the "helicities" h und h', as defined in Eq. (1), have the values ± 1. With these definitions the leptonic matrix element takes the form:

$$\Omega_{h,\lambda} = \left\{ -\frac{\lambda}{\sqrt{2}} \left[\sqrt{\frac{1+\epsilon}{1-\epsilon}} + h\lambda \right] + \sqrt{\frac{2\epsilon}{1-\epsilon}} \delta_{\lambda 0} \right\} Q . \tag{47}$$

In deriving this equation, the following relations are useful:

$$\sin\frac{\Theta}{2} = \frac{Q}{2\sqrt{E'E}} ,$$
$$\cos\frac{\Theta}{2} = \sqrt{\frac{2\epsilon}{1-\epsilon}} \frac{q}{Q} \sin\frac{\Theta}{2} ,$$
$$\sin\left(\frac{\Theta_1 + \Theta_2}{2}\right) = \sqrt{\frac{1+\epsilon}{1-\epsilon}} \sin\frac{\Theta}{2} . \tag{48}$$

We now return to the hadronic matrix element in Eq. (40) and assume that the target nucleon is fully polarized in the direction

$$\hat{P} = (\sin\Psi\cos\Phi,\ \sin\Psi\sin\Phi,\ \cos\Psi) = (P_x,\ P_y,\ P_z) . \tag{49}$$

In general the nucleon is therefore in a superposition of states with definite helicity,

$$|N\rangle = \cos\frac{\Psi}{2}|\tfrac{1}{2},\tfrac{1}{2}\rangle + e^{i\Phi}\sin\frac{\Psi}{2}|\tfrac{1}{2},-\tfrac{1}{2}\rangle . \tag{50}$$

Equation (40) involves transitions for all values of λ, Λ, and $\Lambda' = \lambda + \Lambda$, which gives 6 different matrix elements. However, the helicity amplitudes obey the relation

$$\langle J, -\Lambda'|\varepsilon^{(-\lambda)} \cdot J|\tfrac{1}{2}, -\Lambda\rangle = \xi\langle J, \Lambda'|\varepsilon^{(\lambda)} \cdot J|\tfrac{1}{2}, \Lambda\rangle , \tag{51}$$

i.e., the sign reversal of all the involved helicities only leads to an overall phase, $|\xi| = 1$. Moreover, with an appropriate definition of the wave functions, all helicity amplitudes turn out to be real, and therefore $\xi = \pm 1$. While the phase ξ depends on the quark wave function of the respective resonance, it has the same value for all 3 components of the current. We can therefore relate all hadronic matrix elements to the 3 helicity amplitudes of Eq. (22) and the phase ξ. Equation (40) can now be cast into the form:

$$\begin{aligned}
T_{\Lambda' h' \Lambda h} \sim\ & \Omega_{h,0}\left(\cos\frac{\Psi}{2}\,\delta_{\Lambda',\frac{1}{2}}\delta_{\Lambda,\frac{1}{2}} + e^{i\Phi}\sin\frac{\Psi}{2}\,\delta_{\Lambda',-\frac{1}{2}}\delta_{\Lambda,-\frac{1}{2}}\,\xi\right)\frac{Q}{q}S_{\frac{1}{2}} \\
+\ & \Omega_{h,1}\left(\cos\frac{\Psi}{2}\,A_{\frac{3}{2}}\delta_{\Lambda',\frac{3}{2}}\delta_{\Lambda,\frac{1}{2}} + e^{i\Phi}\sin\frac{\Psi}{2}\,A_{\frac{1}{2}}\delta_{\Lambda',\frac{1}{2}}\delta_{\Lambda,-\frac{1}{2}}\right) \tag{52}\\
+\ & \Omega_{h,-1}\left(\cos\frac{\Psi}{2}\,\xi\,A_{\frac{1}{2}}\delta_{\Lambda',-\frac{1}{2}}\delta_{\Lambda,\frac{1}{2}} + e^{i\Phi}\sin\frac{\Psi}{2}\,\xi\,A_{\frac{3}{2}}\delta_{\Lambda',-\frac{3}{2}}\delta_{\Lambda,-\frac{1}{2}}\right) .
\end{aligned}$$

In order to derive the cross section, we sum the absolute squares of the matrix elements over the final state helicities:

$$
\begin{aligned}
\sum_{h',\Lambda'} |T_{h'\Lambda'h\Lambda}|^2 \quad &\sim \quad |\Omega_{h,0} \cos\tfrac{\Psi}{2} \tfrac{Q}{q} S_{\frac{1}{2}} + \Omega_{h,1} e^{i\Phi} \sin\tfrac{\Psi}{2} A_{\frac{1}{2}}|^2 \\
&+ \quad |\Omega_{h,0} e^{i\Phi} \sin\tfrac{\Psi}{2} \xi\tfrac{Q}{q} S_{\frac{1}{2}} + \Omega_{h,-1} \cos\tfrac{\Psi}{2} \xi A_{\frac{1}{2}}|^2 \\
&+ \quad |\Omega_{h,1} \cos\tfrac{\Psi}{2} A_{\frac{3}{2}}|^2 + |\Omega_{h,-1} e^{i\Phi} \sin\tfrac{\Psi}{2} \xi A_{\frac{3}{2}}|^2 . \quad (53)
\end{aligned}
$$

It is now evident that the state-dependent phase ξ drops out in the inclusive cross section. Therefore, the above equation can be cast into the form:

$$
\begin{aligned}
\sum_{h',\Lambda'} |T_{h'\Lambda'h\Lambda}|^2 \quad &\sim \quad \epsilon\frac{Q^2}{q^2} |S_{\frac{1}{2}}|^2 + \frac{1}{2}(1 - \cos\Psi\sqrt{1-\epsilon^2}) |A_{\frac{1}{2}}|^2 \\
&+ \quad \frac{1}{2}(1 + \cos\Psi\sqrt{1-\epsilon^2}) |A_{\frac{3}{2}}|^2 \\
&- \quad \sin\Psi\cos\Phi\, h\sqrt{2\epsilon(1-\epsilon)}\frac{Q}{\sqrt{2}\,q} \operatorname{Re}(S_{\frac{1}{2}}^* A_{\frac{1}{2}}) \\
&- \quad \sin\Psi\sin\Phi\sqrt{2\epsilon(1+\epsilon)}\frac{Q}{\sqrt{2}\,q} \operatorname{Im}(S_{\frac{1}{2}}^* A_{\frac{1}{2}}) . \quad (54)
\end{aligned}
$$

The last term in this equation must vanish in the inclusive cross section, see Eq.(1). This requires that $S_{\frac{1}{2}}^* A_{\frac{1}{2}}$ is a real number, which is of course also the case in any quark model calculation. In the following we shall therefore treat the helicity amplitudes as real numbers. Our final result takes the following form:

$$
\begin{aligned}
\sum_{h',\Lambda'} |T_{h'\Lambda'h\Lambda}|^2 \quad &\sim \quad \frac{1}{2}(A_{\frac{1}{2}}^2 + A_{\frac{3}{2}}^2) + \epsilon\frac{Q^2}{q^2} S_{\frac{1}{2}}^2 \\
&- \quad h\, P_z \sqrt{1-\epsilon^2}\frac{1}{2}(A_{\frac{1}{2}}^2 - A_{\frac{3}{2}}^2) \\
&- \quad h\, P_x \sqrt{2\epsilon(1-\epsilon)}\frac{Q}{\sqrt{2}\,q} S_{\frac{1}{2}} A_{\frac{1}{2}} , \quad (55)
\end{aligned}
$$

with $P_z = \cos\Psi$, $P_x = \sin\Psi\cos\Phi$, and independent of P_y. Comparing finally with Eq.(1) we find, up to a common factor, the results of Eq.(27),

$$
\sigma_T \sim \frac{1}{2}(A_{\frac{1}{2}}^2 + A_{\frac{3}{2}}^2) \quad , \quad \sigma_{TT} \sim \frac{1}{2}(A_{\frac{1}{2}}^2 - A_{\frac{3}{2}}^2) ,
$$

$$
\sigma_L \sim \frac{Q^2}{q^2} S_{\frac{1}{2}}^2 \quad , \quad \sigma_{LT} \sim -\frac{Q}{\sqrt{2}\,q} S_{\frac{1}{2}} A_{\frac{1}{2}} . \quad (56)
$$

References

[1] D. Drechsel, B. Pasquini, M. Vanderhaeghen Phys. Rept. 378 (2003) 99.

[2] D. Drechsel, L. Tiator, Annu. Rev. Nucl. Part. Sci. **54** (2004) in press.

[3] J. Ahrens et al. (GDH and A2 Collaboration), Phys. Rev. Lett. **84** (2000) 5950.

[4] K. Abe et al. (E143 Collaboration), Phys. Rev. **D 58** (1998) 112003.

[5] A. Airapetian et al. (HERMES Collaboration), Eur. Phys. J. **C26** (2003) 527.

[6] R. Fatemi et al. (CLAS collaboration), Phys. Rev. Lett. **91** (2003) 222002.

[7] M. Amarian et al. (JLab E94010 collaboration), Phys. Rev. Lett. **89** (2002) 242301.

[8] M. Amarian et al. (JLab E94010 collaboration), Phys. Rev. Lett. **92** (2004) 022301.

[9] D. Drechsel, O. Hanstein, S. Kamalov, L. Tiator, Nucl. Phys. **A 645** (1999) 145.

[10] D. Drechsel, S. Kamalov, L. Tiator, Phys. Rev. **D 63** (2001) 114010.

[11] L.A. Copley, G. Karl, E. Obryk, Phys. Lett. **29** (1969) 117; N. Isgur, G. Karl, Phys. Rev. **D18** (1978) 4187, Phys. Rev. **D19** (1979) 2653, Phys. Rev. **D20** (1979) 1191; R. Koniuk, N. Isgur, Phys. Rev. **D21** (1980) 1868.

[12] S. Capstick, N. Isgur, Phys. Rev. **D 34** (1986) 2809.

[13] L. Ya. Glozman, D.O. Riska, Phys. Rep. **268** (1996) 263.

[14] L. Ya. Glozman, Z. Papp, W. Plessas, K. Varga R. F. Wagenbrunn, Phys. Rev. **C57** (1998) 3406; L. Ya. Glozman, W. Plessas, K. Varga, R. F. Wagenbrunn, Phys. Rev. **D58** (1998) 094030.

[15] R. Bijker, F. Iachello, A. Leviatan, Ann. Phys. (N.Y.) **236** (1994) 69.

[16] M. Ferraris, M.M. Giannini, M. Pizzo, E. Santopinto, L. Tiator, Phys. Lett. **B 364** (1995) 231.

[17] M. Aiello, M. Ferraris, M.M. Giannini, M. Pizzo, E. Santopinto, Phys. Lett. **B 387** (1996) 215.

[18] M. Aiello, M.M. Giannini, E. Santopinto, J. Phys. G: Nucl. Part. Phys. **24** (1998) 753.

[19] M. De Sanctis, M.M. Giannini, E. Santopinto, Eur. Phys. J. **A 2** (1998) 403.

[20] M.M. Giannini and E. Santopinto, Few Body Systems Suppl. **11** (1999) 37.

[21] D. Drechsel and M.M. Giannini, Few Body Systems **15** (1993) 99; M. De Sanctis, D. Drechsel, and M.M. Giannini, Few Body Systems **16** (1994) 143; Z. Li, Phys. Rev. **D 47** (1993) 1854; Z. Li and D. Yu-Bing, Phys. Rev. **D 54** (1996) 4301; D. Drechsel, Prog. Part. Nucl. Phys. **15** (1995) 181; F. Cardarelli, B. Pasquini, and S. Simula, Phys. Lett. **D 418** (1998) 237.

[22] W.X. Ma, D.H. Li, A.W. Thomas, Z.P. Li, Nucl. Phys. **A635** (1998) 497.

[23] A.M. Baldin, Nucl. Phys. **18** (1960) 310, L.I. Lapidus, Sov. Phys. JETP **16** (1963) 964.

[24] S. Gerasimov, Yad. Fiz. **2** (1965) 598 [Sov. J. Nucl. Phys. **2** (1966) 430], S.D. Drell and A.C. Hearn, Phys. Rev. Lett. **16** (1966) 908.

[25] J.D. Bjorken, Phys. Rev. **148** (1966) 1467, Phys. Rev. **D 1** (1970) 1376.

[26] P.L. Anthony *et al.*, (E155 Collaboration) Phys. Lett. **B 493** (2000) 19.

[27] S.A. Larin, J.A.M. Vermaseren, Phys. Lett. **B 259** (1991) 345.

[28] H. Burkhardt, W.N. Cottingham, Ann. Phys. **56** (1970) 453.

[29] Babusci, Giordano, Mattone, Phys. Rev. **C 57** (1998) 291.

[30] G. Bali et al., Phys. Rev. **D51**, 5165 (1995); G. Bali, Phys. Rep. **343** (2001) 1.

[31] P. Hasenfratz, R.R. Hogan, J. Kuti, and J.M. Richard, Phys. Lett. **B 94** (1980) 401.

[32] M. Fabre de la Ripelle and J. Navarro, Ann. Phys. (N.Y.) **123** (1979) 185.

[33] E. Santopinto, F. Iachello, M.M. Giannini, Nucl. Phys. **A623** (1997) 100; Eur. Phys. J. **A1** (1998) 307.

[34] M.M. Giannini and E. Santopinto, to be published.

[35] M.M. Giannini, Rep. Prog. Phys. **54** (1990) 453-529.

[36] V. Burkert, and B.L. Ioffe, Phys. Lett. **B 296** (1992) 223.

[37] J. Blümlein, M. Böttcher, Nucl. Phys. **B 636** (2002) 225.

[38] C. Ciofi degli Atti and S. Scopetta, Phys. Lett. **B 404** (1997) 223.